EasyChair Preprint

№ 15104

Fluorescence Lifetime of NV Centers for Temperature-Insensitive All-Optical Magnetic Field Sensing

Ludwig Horsthemke, Jens Pogorzelski, Dennis Stiegekoetter, Frederik Hoffmann, Ann-Sophie Bülter, Lutz Langguth, Robert Staacke, Sarah Trinschek, Markus Gregor and Peter Gloesekoetter

September 27, 2024

Fluorescence Lifetime of NV Centers for Temperature-Insensitive All-Optical Magnetic Field Sensing

Ludwig Horsthemke*, Jens Pogorzelski*, Dennis Stiegekötter*, Frederik Hoffmann*, Ann-Sophie Bülter*, Lutz Langguth†, Robert Staacke†, Sarah Trinschek‡, Markus Gregor‡, and Peter Glösekötter*
*Department of Electrical Engineering and Computer Science,
FH Münster—University of Applied Sciences, Stegerwaldstr. 39, 48565 Steinfurt, Germany
l.horsthemke@fh-muenster.de
†Quantum Technologies GmbH, Alte Messe 6, 04103 Leipzig, Germany
‡Department of Engineering Physics,
FH Münster—University of Applied Sciences, Stegerwaldstr. 39, 48565 Steinfurt, Germany

***Abstract*—We investigate the combined temperature and magnetic field dependent behavior of high NV-density microdiamonds in an all-optical frequency-domain based setup, utilizing the change in fluorescence lifetime. We use these frequency-domain data to train neural networks for the prediction of temperatures and magnetic fields. At zero magnetic field, we show the ability to predict temperatures in the range of $0\,^{\circ}\mathrm{C}$ to $100\,^{\circ}\mathrm{C}$, with a standard deviation of $1.24\,^{\circ}\mathrm{C}$. Furthermore, we show the ability to predict applied magnetic fields, while varying the ambient temperature. We achieve a higher accuracy, compared to the approach of observing of the fluorescence intensity at a single excitation frequency.**

***Index Terms*—NV center, fluorescence lifetime, all-optical, magnetometry, temperature**

I. All-Optical Magnetic Field Sensing with NV centers

Magnetic field sensing, using negatively charged nitrogen-vacancy (NV) centers has been the focus of many research groups, demonstrating high magnetic sensitivities [1], [2], and high spatial resolutions [3], [4], while operating at room temperature. These setups are commonly based on the manipulation of NV spin states, using resonant microwave (MW) excitation. All MW based systems, however, come with added complexity, originating in the necessary galvanic connection for MW delivery to the sensing volume, and the interaction of MW with the environment [5]. MW-free setups, on the other hand, can overcome these limitations. They may utilize narrow-band features, like the ground-state level anticrossing [6]–[8]. This allows for highly sensitive setups, requiring stable and precisely aligned bias fields, though. Alternatively, all-optical setups may use the fluorescence manipulation through spin mixing for magnetic fields up to $\approx 50\,\mathrm{mT}$ [9], [10], enabling a high magnetic bandwidth, without the need for bias fields. This reduced complexity is a step towards industrial application. An all-optical system can be based on a diamond-tipped optical fiber, allowing the simultaneous excitation of NV centers and collection of fluorescence [10]–[13]. Such a non-magnetic and non-conductive probe realizes high insulation resistances.

A new approach to all-optical sensing is based on the excited state lifetime of NV centers [14], [15]. When the excitation light is intensity modulated and the modulation frequency is swept in a sufficiently high range, the decay dynamics of the fluorescence show a low-pass behavior. With increasing modulation frequency, the fluorescence intensity then decreases and the phase between excitation and fluorescence shows a shift from 0° to 90° [16]. The excited state lifetime components respond to magnetic fields, leading to a change in the associated frequency response [3], [14], [17]. This response may be used to identify suitable excitation frequencies for lock-in amplifier setups, which use a single excitation frequency and monitor either the fluorescence magnitude or phase as a measurement quantity. Alternatively, we can use the complete frequency response to gain more insight into the system's state. For example, we have shown the ability to resolve an ambiguity at a single excitation frequency for low magnetic fields [15].

II. Temperature Dependence in NV-based magnetometry

Temperature sensing with NV-centers is a topic of active research. It is commonly based on the detection of the shift of the zero-field splitting in optically detected magnetic resonance experiments [18]–[23]. These implementations achieve high spatial resolutions, but again come with the limitations of MW delivery.

All-optical approaches for NV-based thermometry are also feasible and usually based on the change of the spectral shape [24], [25]. They rely on the observation of zero-phonon line

Research funded by Bundesministerium für Bildung und Forschung (13N15489 and 13N15971) and by CETPartnership, the Clean Energy Transition Partnership under the 2022 joint call for research proposals, co-funded by the European Commission (GA N°101069750) and with the funding organizations detailed on https://cetpartnership.eu/funding-agencies-and-call-modules (Bundesministerium für Wirtschaft und Klimaschutz 03EI6113A).

(ZPL) shift or intensity change. Also, the ratio of the ZPL to the entire spectrum (i.e. Debye–Waller factor) has been used [26]. This ratiometric approach is a robust solution for temperature measurements because the overall fluorescence intensity can be affected by many environmental factors.

A rise in temperature is accompanied by an overall reduction of the fluorescence intensity [22], [27] and in time-resolved fluorescence spectroscopy a reduction of the fluorescence lifetime with rising temperature has been shown [27], [28]. In an experiment, which only observes the intensity or phase at a fixed excitation frequency, this behavior leads to a temperature-dependent measurement quantity. In contrast, we explore the use of the complete frequency response data for a temperature-insensitive measurement of magnetic fields.

III. Materials and Methods

A. Frequency Domain Measurements

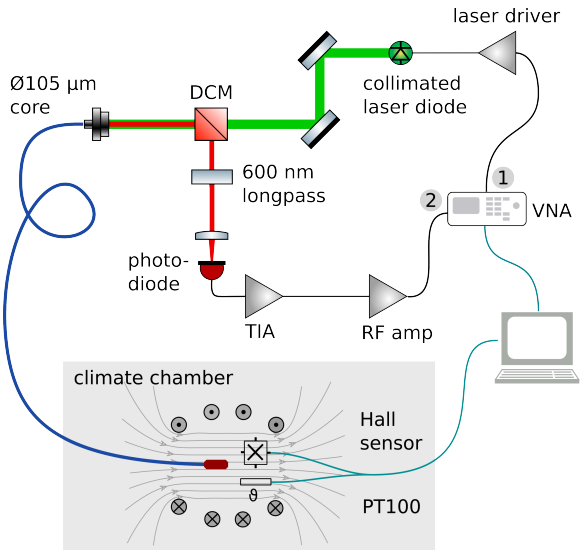

Fig. 1. Schematic of the optical and electrical setup for frequency domain measurements. The fiber tip with NV-rich diamond powder is placed in an electromagnet, which is monitored by a Hall effect sensor and a PT100 temperature probe.

In this work, we investigate a sample of NV-rich diamond powder in a frequency domain fluorescence lifetime measurement at varying temperatures and magnetic fields.

In Figure 1, we show the optical and electrical setup for frequency domain measurements. A varying frequency stimulus from port one of a vector network analyzer (VNA) is passed to a comparator, controlling a laser driver switch (iC-Haus GmbH iC-HKB). The collimated green laser diode (ams-OSRAM PLT5 520B) emits excitation light at a mean optical output power of $12\,\mathrm{mW}$, which is passed through a dichroic mirror (DCM, Thorlabs DMPS567R) and coupled to a $105\,\mu\mathrm{m}$ core diameter fibre. The end facet of the fibre is placed next to high NV-density microdiamonds in a glass cuvette. The amount of microdiamonds is large enough to completely cover the fiber's end facet. The fluorescence is collected via the same fiber, passed through a long-pass filter and focused (Thorlabs FELH600 & LA1951-AB) on a photodiode. The photocurrent is amplified by a transimpedance amplifier ($12\,\mathrm{k\Omega}$, $75\,\mathrm{MHz}$ bandwidth) and passed to port two of the VNA. The VNA sweeps the frequency of the stimulus signal in a range of 1–$100\,\mathrm{MHz}$ and records magnitude and phase relation between the two ports. In each sweep, the VNA records this response at 401 distinct frequencies with a bandwidth of $1\,\mathrm{kHz}$. We record the average of five sweeps for one observation.

An electromagnet, monitored by a Hall effect sensor, is used to apply magnetic fields up to $80\,\mathrm{mT}$. The electromagnet, containing the fiber probe with NV-rich diamond powder, is placed in a climate chamber. We additionally monitor the ambient temperature inside the coil with a PT100 temperature probe.

B. Regression Methods

We use excitation light powers for which we expect no saturation behavior [29], [30]. The fluorescence signal can then be understood as the convolution of the excitation signal with the fluorescence decay dynamics. For our material, we found them to be well explained by a bi-exponential decay [14]. We find the respective frequency domain representation by the Laplace-transform of a sum of two exponential functions

$$H(s) = \frac{a_1}{s + \frac{1}{\tau_1}} + \frac{a_2}{s + \frac{1}{\tau_2}}, \tag{1}$$

with the time constants τ_1, τ_2 and their amplitudes a_1, a_2.

The VNA is calibrated with a system response $H(s)|_0$ at known parameters $B = 0$ and $T = 0\,^\circ\mathrm{C}$. This response contains the transmission behavior of all optical and electrical components, involved in the measurement, as well as the decay dynamics of the fluorescence itself. The VNA then corrects for $H(s)|_0$, resulting in the measurement of

$$H_r(s) = \frac{H(s)|_B}{H(s)|_0}. \tag{2}$$

This ratio has a magnitude of 1 and phase of 0 at $B = 0$ and $T = 0\,^\circ\mathrm{C}$, and we only record the changes by the influence of B and T on the material.

In Figure 2, we show example measurements at different temperatures and magnetic fields. We observe a high magnetic contrast of the magnitude at low frequencies, as well as a high magnetic contrast of the phase around $13\,\mathrm{MHz}$. Under constant magnetic fields and increasing temperatures the magnitude decreases in the whole range of excitation frequencies. Additionally, the phase increases with rising temperatures at low frequencies.

In previous experiments we only varied the magnetic fields and were able to fit Equation 2 to the measurements. With the additional variation of the temperature, we can no longer satisfactorily apply these fits. We therefore employ machine learning algorithms for the regression of these two variables. We aim to investigate, if temperature independent magnetometry can be implemented with the frequency domain approach.

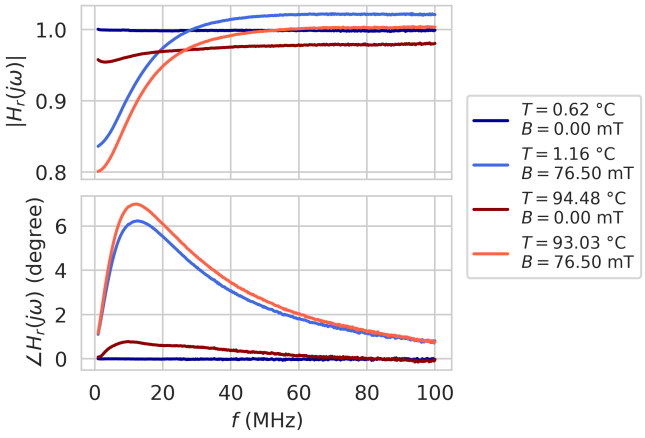

Fig. 2. Measurements of the magnitude $|H_r|$ and phase $\angle H_r$, as functions of the excitation frequency f at different temperatures T and magnetic fields B.

C. Temperature Dependence

At first, we swept the climate chamber's set temperature between 0 °C to 100 °C at zero magnetic field, with each ramp taking one hour. We added dwell times at the extremes of 10 minutes. During 18 sweeps, taking 22 hours, we recorded 18373 frequency responses. We use a neural network for the regression of the temperature from the measurements. Therefore, we implemented a fully connected neural network (FCNN) with three hidden layers, of sizes 95, 65 and 35 nodes, using ReLU activation functions. The output layer is a single node with a linear activation function. Observations consist of the concatenation of magnitude $|H_r|$ and phase $\angle H_r$ at 401 different frequencies, labeled by T. The input layer consists of 802 nodes, accordingly. We split the observations by ratios of 55%, 15%, and 30% into training-, validation- and test-sets, respectively. Also, we fit a MinMaxScaler to the training data and apply it to the whole data set, so observations are scaled per feature to lie within the interval [0,1]. The artificial neural networks are implemented and trained, using TensorFlow [31].

D. Temperature and Magnetic Field Dependence

Next, we swept the chamber's temperature from 0 °C to 80 °C in 8 hours and back to 0 °C in 4 hours. During this time, we continuously swept the magnetic field from 0 mT to 30 mT in 25 steps and further to 80 mT in 15 additional steps. We reduced the number of discrete magnetic field steps at higher values, to limit the additional heating by the electromagnet to 20 K above ambient temperature. During 16 hours, we recorded 6494 frequency responses. For the combined regression of temperatures and magnetic fields from the measurements, we use a FCNN with the same architecture, as in the previous case. We only changed the output layer to two nodes with linear activation functions. We also used the same splits between training-, validation- and test-sets, and applied a MinMaxScaler. The observations are now labeled by T and B.

IV. Results and Discussion

A. Temperature Dependence

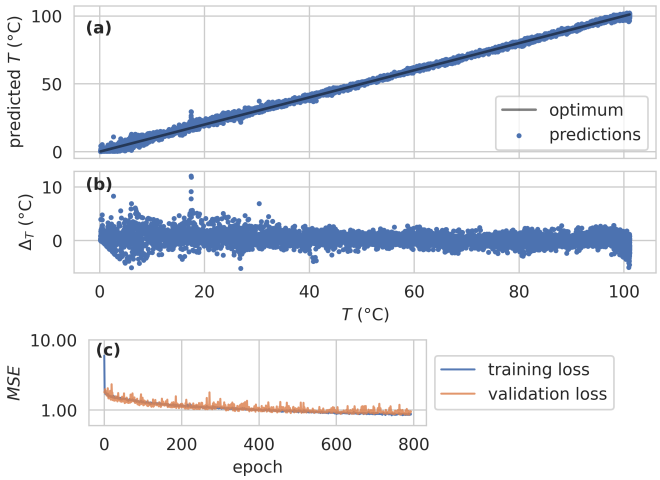

Fig. 3. (**a**) Predictions of the FCNN on the test set in comparison to the optimum linear relationship. (**b**) Differences of predictions in (a) to the linear relation. (**c**) Mean squared error on training and validation sets during training of the FCNN.

In the first experiment, the frequency responses were acquired at varying temperatures and zero magnetic field. A FCNN was trained in 800 epochs, after which the validation loss showed no significant improvement. The loss functions, plotted in Figure 3c, show no signs of overfitting. In Figure 3a, we show the predictions of the FCNN on the test set. For the difference of the prediction to the linear relation Δ_T, we find a mean value of 0.29 °C and a standard deviation of 1.24 °C. These results were consistent over multiple training runs with different randomly chosen subsets for training and test. We observed no significant outliers, showing the temperature can be estimated at zero magnetic field, with 99% of the values of Δ_T lying within ± 3.8 °C.

B. Temperature and Magnetic Field Dependence

In the second experiment, the measurements were acquired at slowly varying temperatures, while sweeping the applied magnetic field in discrete steps up to 76 mT. The Hall effect magnetic field probe showed a temperature dependence of approximately −620 ppm/K, leading to a low accuracy at high temperatures. To obtain more accurate magnetic field labels, the currents at the discrete steps were used. Therefore, we recorded the magnetic field in the electromagnet at $T = 25$ °C with the Hall sensor as a function of current in the electromagnet. A linear fit was then used to calculate magnetic field labels from the actual currents in the electromagnet.

The same network structure as before, except for two output nodes with linear activation functions, was used, to simultaneously predict magnetic fields and temperatures from the observations. We observed no overfitting in over 600 epochs, after which the validation loss stopped to improve. In Figures 4a,b, we show the predictions of temperatures

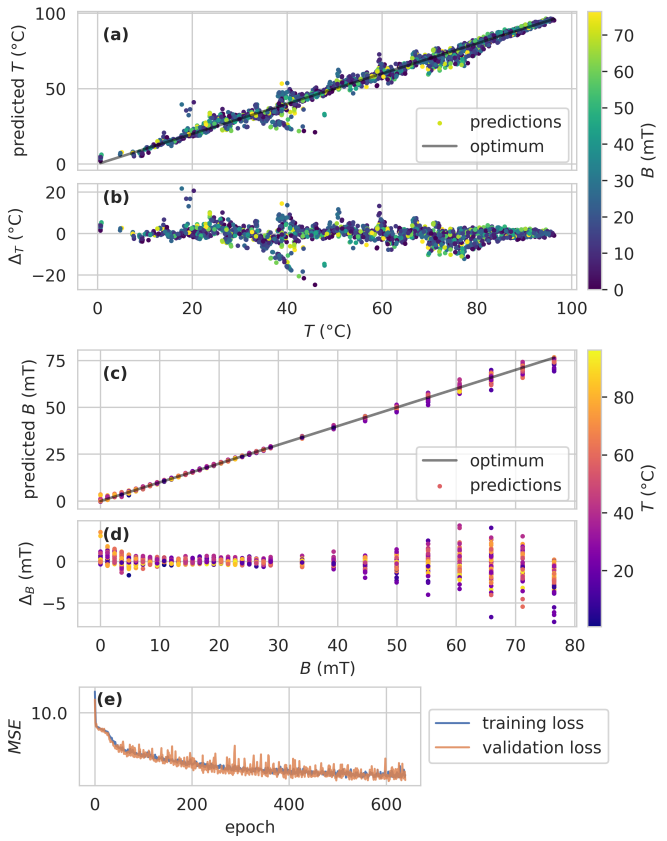

Fig. 4. Combined regression of temperatures and magnetic fields. (**a**) Predictions of temperature on the test set in comparison to the optimum linear relationship. Colors show the respective magnetic field of the observation. (**b**) Differences of predictions in (a) to the linear relation. (**c**) Predictions of magnetic fields on the test set in comparison to the optimum linear relationship. Colors show the respective temperature of the observation. (**d**) Differences of predictions in (c) to the linear relation. (**e**) Mean squared error on training and validation sets during training of the FCNN.

and the differences to a linear relationship, respectively. In comparison to the previous study, we find a higher variance, with outliers up to $\pm 22\,^{\circ}\mathrm{C}$ from the real values. We observe a mean deviation from the linear relation of $-0.15\,^{\circ}\mathrm{C}$ and a standard deviation in Δ_T of $3.63\,^{\circ}\mathrm{C}$. Additionally, the colors indicate the magnetic fields, which are associated with the observations. This allows us to visualize potential clusters of magnetic fields, which might lead to observations with higher error in the predictions. However, we see no such clusters.

Figures 4c,d show the same predictions, with respect to magnetic fields. We find a mean deviation from a linear behavior of $-0.13\,\mathrm{mT}$ at a standard deviation of $0.79\,\mathrm{mT}$. Additionally, 99% of the values of Δ_B lie within $\pm 3.27\,\mathrm{mT}$, showing the ability to predict magnetic fields, insensitive to varying sample temperatures. We observe a higher variance at high magnetic fields. This may be a consequence of the lower number of observations at these fields. We use colors to show the temperatures, associated with the predictions and their underlying observations. We see no correlation of the error with certain temperature ranges.

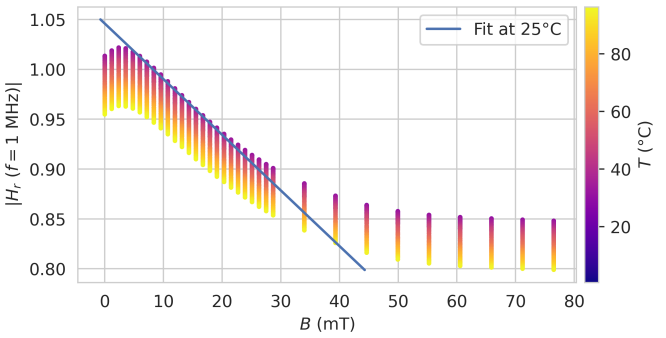

Fig. 5. Fluorescence intensity at excitation frequency $f = 1\,\mathrm{MHz}$ as a function of magnetic field and temperature. The linear fit was applied to the data at $25\,^{\circ}\mathrm{C}$ in the range of $10\,\mathrm{mT}$ to $20\,\mathrm{mT}$.

For an implementation, only observing the fluorescence intensity at one fixed excitation frequency, we can estimate the error, introduced by varying temperatures. In Figure 5, we show the fluorescence intensity at the lowest excitation frequency $|H_r(f = 1\,\mathrm{MHz})|$ as a function of the magnetic field in the tested temperature range. We apply a linear fit to the data at $25\,^{\circ}\mathrm{C}$ in the range of $10\,\mathrm{mT}$ to $20\,\mathrm{mT}$. The fit is then used, to calculate the magnetic fields from the data at nominally $15.5\,\mathrm{mT}$. The resulting magnetic field values would span a range of $9\,\mathrm{mT}$ and show a standard deviation of $2.73\,\mathrm{mT}$. The observation of the phase at a fixed excitation frequency would lead to similar values. In contrast, in our solution, the predicted magnetic field at nominally $15.5\,\mathrm{mT}$ spans a range of $370\,\mu\mathrm{T}$ for the recorded temperature range and shows a standard deviation of only $120\,\mu\mathrm{T}$.

V. Conclusion

In this work we investigated the combined temperature and magnetic field dependent behavior of high NV-density microdiamonds in an all-optical frequency-domain based setup, utilizing the change in fluorescence lifetime. At zero magnetic field, we have shown the ability to predict temperatures in the range of $0\,^{\circ}\mathrm{C}$ to $100\,^{\circ}\mathrm{C}$, with a standard deviation of $1.24\,^{\circ}\mathrm{C}$. Furthermore, we have shown the ability to predict applied magnetic fields, while varying the ambient temperature, with a higher accuracy, compared to the sole observation of the fluorescence intensity at a single excitation frequency. With the recent development of low-cost VNAs [32], [33], this work shows a step towards temperature-insensitive industrial application of all-optical NV-based magnetometry.

References

[1] J. F. Barry, J. M. Schloss, E. Bauch, M. J. Turner, C. A. Hart, L. M. Pham, and R. L. Walsworth, "Sensitivity optimization for NV-diamond magnetometry," *Reviews of Modern Physics*, vol. 92, no. 1, p. 015004, mar 2020.

[2] Y. Xie, H. Yu, Y. Zhu, X. Qin, X. Rong, C.-K. Duan, and J. Du, "A hybrid magnetometer towards femtotesla sensitivity under ambient conditions," *Science Bulletin*, vol. 66, no. 2, pp. 127–132, Jan. 2021.

[3] J.-P. Tetienne, L. Rondin, P. Spinicelli, M. Chipaux, T. Debuisschert, J.-F. Roch, and V. Jacques, "Magnetic-field-dependent photodynamics of single NV defects in diamond: an application to qualitative all-optical magnetic imaging," *New Journal of Physics*, vol. 14, no. 10, p. 103033, oct 2012.

[4] T. X. Zhou, R. J. Stöhr, and A. Yacoby, "Scanning diamond nv center probes compatible with conventional afm technology," *Applied Physics Letters*, vol. 111, no. 16, Oct. 2017.

[5] I. S. Maksymov and M. Kostylev, "Impact of eddy currents on the dispersion relation of surface spin waves in thin conducting magnetic films," *Journal of Physics D: Applied Physics*, vol. 46, no. 49, p. 495001, nov 2013. [Online]. Available: https://doi.org/10.1088%2F0022-3727%2F46%2F49%2F495001

[6] A. Wickenbrock, H. Zheng, L. Bougas, N. Leefer, S. Afach, A. Jarmola, V. M. Acosta, and D. Budker, "Microwave-free magnetometry with nitrogen-vacancy centers in diamond," *Applied Physics Letters*, vol. 109, no. 5, p. 053505, 2016. [Online]. Available: https://doi.org/10.1063/1.4960171

[7] H. Zheng, G. Chatzidrosos, A. Wickenbrock, L. Bougas, R. Lazda, A. Berzins, F. H. Gahbauer, M. Auzinsh, R. Ferber, and D. Budker, "Level anti-crossing magnetometry with color centers in diamond," 2017.

[8] H. Zheng, Z. Sun, G. Chatzidrosos, C. Zhang, K. Nakamura, H. Sumiya, T. Ohshima, J. Isoya, J. Wrachtrup, A. Wickenbrock, and D. Budker, "Microwave-free vector magnetometry with nitrogen-vacancy centers along a single axis in diamond," *Phys. Rev. Applied*, vol. 13, p. 044023, Apr 2020. [Online]. Available: https://link.aps.org/doi/10.1103/PhysRevApplied.13.044023

[9] R. Staacke, R. John, R. Wunderlich, L. Horsthemke, W. Knolle, C. Laube, P. Glösekötter, B. Burchard, B. Abel, and J. Meijer, "Isotropic scalar quantum sensing of magnetic fields for industrial application," *Advanced Quantum Technologies*, vol. n/a, no. n/a, p. 2000037, 2020. [Online]. Available: https://doi.org/10.1002/qute.202000037

[10] I. Fedotov, L. Amitonova, D. Sidorov-Biryukov, N. Safronov, S. Blakley, A. Levchenko, S. Zibrov, A. Fedotov, S. Kilin, M. Scully, V. Velichansky, and A. Zheltikov, "Fiber-optic magnetic-field imaging," *Optics Letters*, vol. 39, 12 2014.

[11] D. Duan, G. X. Du, V. K. Kavatamane, S. Arumugam, Y.-K. Tzeng, H.-C. Chang, and G. Balasubramanian, "Efficient nitrogen-vacancy centers' fluorescence excitation and collection from micrometer-sized diamond by a tapered optical fiber in endoscope-type configuration," *Optics Express*, vol. 27, no. 5, p. 6734, Feb. 2019.

[12] G. Chatzidrosos, J. S. Rebeirro, H. Zheng, M. Omar, A. Brenneis, F. M. Stürner, T. Fuchs, T. Buck, R. Rölver, T. Schneemann, P. Blümler, D. Budker, and A. Wickenbrock, "Fiberized diamond-based vector magnetometers," *Frontiers in Photonics*, vol. 2, aug 2021.

[13] R. Wunderlich, R. Staacke, W. Knolle, B. Abel, and J. Meijer, "Magnetic field and angle-dependent photoluminescence of a fiber-coupled nitrogen vacancy rich diamond," *Journal of Applied Physics*, vol. 130, no. 12, p. 124901, sep 2021.

[14] L. Horsthemke, J. Pogorzelski, D. Stiegekötter, F. Hoffmann, L. Langguth, R. Staacke, C. Laube, W. Knolle, M. Gregor, and P. Glösekötter, "Excited-state lifetime of nv centers for all-optical magnetic field sensing," *Sensors*, vol. 24, no. 7, p. 2093, Mar. 2024.

[15] L. Horsthemke, J. Pogorzelski, D. Stiegekötter, F. Hoffmann, A.-S. Bülter, S. Trinschek, M. Gregor, and P. Glösekötter, "Towards resolving the ambiguity in low-field, all-optical magnetic field sensing with high nv-density diamonds," in *ITISE 2024*, ser. ITISE 2024. MDPI, Jul. 2024.

[16] J. R. Lakowicz, *Principles of fluorescence spectroscopy*, third edition, corrected at 4. printing ed. New York, NY: Springer, 2010.

[17] N. D. Lai, D. Zheng, F. Jelezko, F. Treussart, and J.-F. Roch, "Influence of a static magnetic field on the photoluminescence of an ensemble of nitrogen-vacancy color centers in a diamond single-crystal," *Applied Physics Letters*, vol. 95, no. 13, p. 133101, sep 2009.

[18] M. W. Doherty, V. M. Acosta, A. Jarmola, M. S. J. Barson, N. B. Manson, D. Budker, and L. C. L. Hollenberg, "Temperature shifts of the resonances of the nv-center in diamond," *Physical Review B*, vol. 90, no. 4, p. 041201, Jul. 2014.

[19] M. Fujiwara and Y. Shikano, "Diamond quantum thermometry: from foundations to applications," *Nanotechnology*, vol. 32, no. 48, p. 482002, Sep. 2021.

[20] V. M. Acosta, E. Bauch, M. P. Ledbetter, A. Waxman, L.-S. Bouchard, and D. Budker, "Temperature dependence of the nitrogen-vacancy magnetic resonance in diamond," *Physical Review Letters*, vol. 104, no. 7, p. 070801, Feb. 2010.

[21] M. Attrash, O. Shtempluck, and E. Buks, "High temperature spectroscopy of ensembles of nitrogen-vacancy centers in diamond," *Journal of Applied Physics*, vol. 133, no. 9, p. 094401, 03 2023. [Online]. Available: https://doi.org/10.1063/5.0128069

[22] M. Fujiwara, S. Sun, A. Dohms, Y. Nishimura, K. Suto, Y. Takezawa, K. Oshimi, L. Zhao, N. Sadzak, Y. Umehara, Y. Teki, N. Komatsu, O. Benson, Y. Shikano, and E. Kage-Nakadai, "Real-time nanodiamond thermometry probing in vivo thermogenic responses," *Science Advances*, vol. 6, no. 37, sep 2020.

[23] Z. Zhang, H. F. Wen, L. Li, B. Cao, Y. Liu, H. Guo, Z. h. Li, Z. Ma, X. Li, J. Tang, and J. Liu, "Temperature dependence of magnetic sensitivity in ensemble nv centers," *Japanese Journal of Applied Physics*, vol. 63, no. 6, p. 062001, Jun. 2024.

[24] T. Plakhotnik, H. Aman, and H.-C. Chang, "All-optical single-nanoparticle ratiometric thermometry with a noise floor of 0.3 k hz-1/2," *Nanotechnology*, vol. 26, no. 24, p. 245501, may 2015. [Online]. Available: https://dx.doi.org/10.1088/0957-4484/26/24/245501

[25] M. Fukami, C. Yale, P. Andrich, X. Liu, F. Heremans, P. Nealey, and D. Awschalom, "All-optical cryogenic thermometry based on nitrogen-vacancy centers in nanodiamonds," *Physical Review Applied*, vol. 12, no. 1, p. 014042, Jul. 2019.

[26] B. Dong, C. Shi, Z. Xu, K. Wang, H. Luo, F. Sun, P. Wang, E. Wu, K. Zhang, J. Liu, Y. Song, and Y. Fan, "Temperature dependence of optical centers in ib diamond characterized by photoluminescence spectra," *Diamond and Related Materials*, vol. 116, p. 108389, Jun. 2021.

[27] T. Plakhotnik and D. Gruber, "Luminescence of nitrogen-vacancy centers in nanodiamonds at temperatures between 300 and 700 k: perspectives on nanothermometry," *Physical Chemistry Chemical Physics*, vol. 12, no. 33, p. 9751, 2010.

[28] D. K. Bommidi and A. D. Pickel, "Temperature-dependent excited state lifetimes of nitrogen vacancy centers in individual nanodiamonds," *Applied Physics Letters*, vol. 119, no. 25, Dec. 2021.

[29] T.-L. Wee, Y.-K. Tzeng, C.-C. Han, H.-C. Chang, W. Fann, J.-H. Hsu, K.-M. Chen, and Y.-C. Yu, "Two-photon excited fluorescence of nitrogen-vacancy centers in proton-irradiated type ib diamond," *The Journal of Physical Chemistry A*, vol. 111, no. 38, pp. 9379–9386, Aug. 2007.

[30] S. Magaletti, L. Mayer, J.-F. Roch, and T. Debuisschert, "A quantum radio frequency signal analyzer based on nitrogen vacancy centers in diamond," *Communications Engineering*, vol. 1, no. 1, Jul. 2022.

[31] M. Abadi, A. Agarwal, P. Barham, E. Brevdo, Z. Chen, C. Citro, G. S. Corrado, A. Davis, J. Dean, M. Devin, S. Ghemawat, I. Goodfellow, A. Harp, G. Irving, M. Isard, Y. Jia, R. Jozefowicz, L. Kaiser, M. Kudlur, J. Levenberg, D. Mané, R. Monga, S. Moore, D. Murray, C. Olah, M. Schuster, J. Shlens, B. Steiner, I. Sutskever, K. Talwar, P. Tucker, V. Vanhoucke, V. Vasudevan, F. Viégas, O. Vinyals, P. Warden, M. Wattenberg, M. Wicke, Y. Yu, and X. Zheng, "TensorFlow: Large-scale machine learning on heterogeneous systems," 2015, software available from tensorflow.org. [Online]. Available: https://www.tensorflow.org/

[32] A. Depold, S. Erhardt, R. Weigel, and F. Lurz, "A 10 khz to 6 ghz low-cost vector network analyzer," *Advances in Radio Science*, vol. 19, pp. 17–22, Dec. 2021.

[33] J. Verhaevert and P. Van Torre, "A low-cost vector network analyzer: Design and realization," in *Loughborough Antennas; Propagation Conference (LAPC 2017)*. Institution of Engineering and Technology, 2017.